Accepted Manuscript

Title: Ultra-thin bimetallic alloy nanowires with porous architecture/monolayer MoS_2 nanosheet as a highly sensitive platform for the electrochemical assay of hazardous omethoate pollutant

Authors: Dandan Song, Qian Li, Xiong Lu, Yanshan Li, Yan Li, Yuanzhe Wang, Faming Gao

PII: S0304-3894(18)30461-8
DOI: https://doi.org/10.1016/j.jhazmat.2018.06.021
Reference: HAZMAT 19458

To appear in: *Journal of Hazardous Materials*

Received date: 25-1-2018
Revised date: 7-6-2018
Accepted date: 9-6-2018

Please cite this article as: Song D, Li Q, Lu X, Li Y, Li Y, Wang Y, Gao F, Ultra-thin bimetallic alloy nanowires with porous architecture/monolayer MoS_2 nanosheet as a highly sensitive platform for the electrochemical assay of hazardous omethoate pollutant, *Journal of Hazardous Materials* (2018), https://doi.org/10.1016/j.jhazmat.2018.06.021

Ultra-thin bimetallic alloy nanowires with porous architecture/monolayer MoS_2 nanosheet as a highly sensitive platform for the electrochemical assay of hazardous omethoate pollutant

Dandan Song, Qian Li, Xiong Lu, Yanshan Li, Yan Li, Yuanzhe Wang, Faming Gao*

Key Laboratory of Applied Chemistry, Department of Applied Chemistry, Yanshan University, Qinhuangdao 066004, P. R. China.

* Corresponding Author E-mail: gaofaming@ysu.edu.cn. Phone: 86 335 8387552. Fax: 86 335 8061569

Graphical Abstract

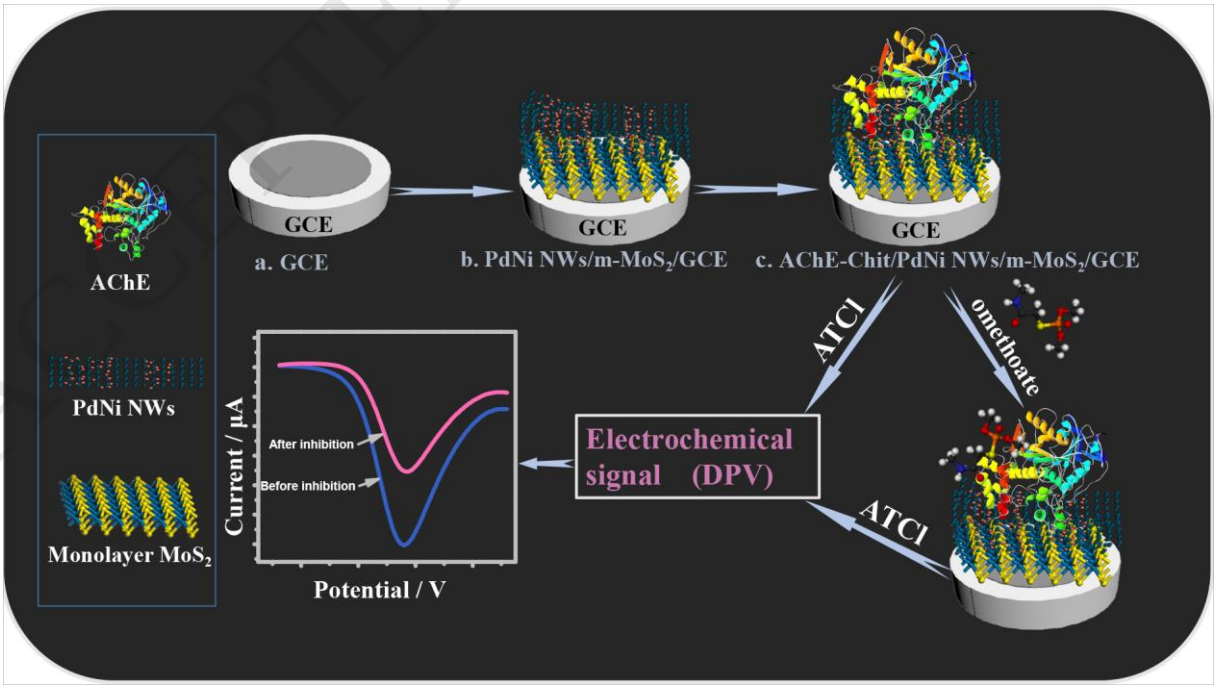

Highlights

- A novel sensing platform is constructed based on the bimetallic alloy ultra-thin NWs/m-MoS_2 nanocomposite.
- The AChE-Chit/PdNi NWs/m-MoS_2/GCE biosensor shows a low detection limit (0.05 pM) for omethoate.
- This biosensor shows high sensitivity, long-time stability and good recoveries (90.4%-96.1%).

Abstract:

A novel electrochemical biosensor was designed for sensitive detection of organophosphate pesticides based on three-dimensional porous bimetallic alloy architecture with ultrathin nanowires (PdCo NWs, PdCu NWs, PdNi NWs) and monolayer MoS_2 nanosheet (m-MoS_2). The bimetallic alloy NWs/m-MoS_2 nanomaterials were used as a sensing platform for electrochemical analysis of omethoate, a representative organophosphate pesticide, via acetylcholinesterase inhibition pathway. We demonstrated that all three bimetallic alloy NWs enhanced electrochemical responses of enzymatic biosensor, benefited from bimetallic synergistic action and porous structure. In particular, PdNi NWs outperformed other two bimetallic alloy. Moreover, PdNi NWs/m-MoS_2 as an electronic transducer is superior to the corresponding biosensor in the absence of monolayer MoS_2 nanosheet, which arise from synergistic signal amplification effect between different components. Under optimized conditions, the developed biosensor on the basis of PdNi NWs/m-MoS_2 shows outstanding performance for the electrochemical assay of omethoate, such as a wide linear range (10^{-13} M~10^{-7} M), a low detection limit of 0.05 pM at a signal-to-noise ratio of 3, high sensitivity and long-time stability. The results demonstrate that bimetallic alloy NWs/m-MoS_2 nanocomposites could be excellent

transducers to promote electron transfer for the electrochemical reactions, holding great potentials in the construction of current and future biosensing devices.

Keywords:

Monolayer MoS_2, bimetallic alloy nanowires, organophosphate pesticides, AChE biosensors

Introduction

Pesticides and their metabolites are routinely leeched into environment as a result of widespread usage on agricultural production [1,2]. These environmental contaminants have posed overwhelming threats to both human and ecosystems health on account of their high toxicity [3,4]. Organophosphate pesticides (OPs) such as omethoate could irreversibly inhibit the activity of acetylcholinesterase (AChE) to exert toxic effects, by binding to the active site of the enzyme [5-7]. AChE is an important enzyme associated with the activity of the nervous system. Long-term exposure to elevated levels of toxic pesticide residues could trigger human nervous system disorders, and even possibly cause organ failure and death [8-11]. Therefore, great attentions have been paid to the analysis of pesticide residues. The current established analytical techniques including gas chromatography/mass spectrometry, high performance liquid chromatography/mass spectrometry and fluorescent bioprobes, are widely considered to be highly sensitive and accurate for the determination of pesticides [12-14]. Nevertheless, these methods suffer from several disadvantages, such as requirements of expensive and sophisticated instruments, complex sample pretreatment process, and sometimes could not be applied for on site and real-time detection. Alternatively, AChE-based biosensors have been designed as an effective method for rapid detection of pesticides in foods and environment [15-20].

Two-dimensional (2D) transition metal dichalcogenides (TMDs) as an emerging class of layered materials, have triggered great interests in many fields, on account of

their ultrathin 2D structure (single- or few-atomic layers) and unique physicochemical properties [21-24]. In comparision with their bulk counterparts, atomically-thin 2D TMDs forms show the enhanced chemical properties with increased surface area and tunable electronic properties, making it desirable for a wide range of applications in field effect transistors, lithium- and sodium-ion batteries, capacitors, and sensors [25-27]. As a representative TMD, molybdenum disulfide (MoS_2) has been discovered to be a promising and superb layered nanomaterial in the field of electrochemical biosensing [28-31]. 2D MoS_2 composed of monolayer or few-layer of S–Mo–S sandwich layers, possesses different numbers of d-electrons, filling up the nonbonding d bands to different levels, resulting in varied electronic properties [32]. More intriguing, 2D MoS_2 has large specific surface area, exceptional biocompatibility, electrochemical activity and easy to functionalization, and particularly it was ultra-sensitive to the changes from surrounding environment [33,34]. Hence, to a great extent, 2D MoS_2 would be an excellent supporting material to fabricate sensitive electrochemical biosensors.

Nanowires (NWs) composed by noble metals (e.g., gold, silver, palladium) have played an important role in electrochemical sensing, due to their intrinsic advantages, such as tremendous surface area-to-volume ratio, excellent biocompatibility, good electrical conductivity and long-time stability [35,36]. Incorporation of transition metals of Co, Ni, and Cu etc. into Pd nanostructures has been proved to effectively enhance the electrochemical activity, which ascribed to synergistic effect and electronic effect in the bimetallic structures [37-42]. Hence, bimetallic alloy NWs as transducers are anticipated to achieve improved sensing performance. Furthermore, when combined with an appropriate supporting material, these bimetallic alloy NWs could show highly enhanced electrochemical activity and stability. Monolayer MoS_2 nanosheet, as an ultra-thin supporting material, has great potentials to make a hybrid nanostructure for enhanced electrochemical sensing performance. Although a large number of research has focused on MoS_2 nanosheets as biosensor platform, monolayer MoS_2 nanosheet in combination with ultra-thin bimetallic alloy NWs has never been proposed and applied for the electrochemical assay of organophosphate pesticides.

With these in mind, ultra-thin bimetallic alloy NWs (PdCu NWs, PdCo NWs, PdNi NWs) with three-dimensional porous architecture were prepared and equipped with monolayer MoS_2 nanosheet as a novel sensing interface. Based on enzymatic inhibition theory, this platform was used for electrochemical assay of omethoate, a high-toxic organophosphate pesticide. The fabrication process of the AChE biosensor for omethoate assay is shown in Scheme 1. The combination of these two nanomaterials is expected to realize synergistic signal amplification and thus enhance electrochemical responses of the AChE biosensor. Besides that, the nanomaterials could provide exceptional large surface area for the electrochemical reactions on the electrodes, which improves the performance of the biosensor. Especially to deserve to be mentioned, 2D MoS_2 was ultra-sensitive to the changes from surrounding environment, which significantly ameliorate the sensitivity of biosensor. Henceforth, we aim to construct a highly sensitive and effective biosensor based on bimetallic

alloy NWs and monolayer MoS_2.

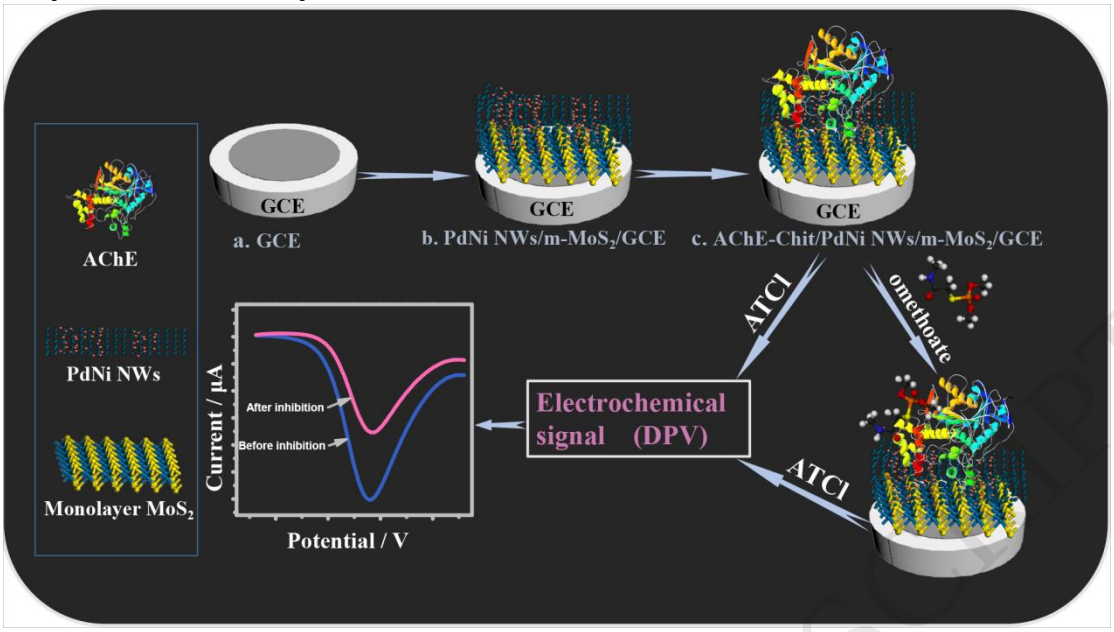

Scheme 1. Schematic illustration of the fabrication process of the AChE biosensor for omethoate assay

2. Experimental section

2.1. Materials and Apparatus.

Acetylcholinesterase (AChE; Type VI-S, lyophilized powder, 500 units/mg protein) from Electrophorus electricus (electric eel), acetylthiocholine chloride, palladium(II) acetylacetonate ($Pd(acac)_2$), nickel(II) acetylacetonate ($Ni(acac)_2$), cobalt(II) acetylacetonate ($Co(acac)_2$), $Cu(NO_3)_2{\cdot}3H_2O$, Triton X-114 and Sodium borohydride ($NaBH_4$) were purchased from Sigma-Aldrich (USA). Omethoate, ≥ 95% purity, was purchased from LGC Promochem (Wesel, Germany). Phosphate buffered saline (PBS, 0.1 M, pH 7.4) was prepared by proportionally mixing of NaH_2PO_4 and Na_2HPO_4 solutions. AChE (0.2 U/μL) was prepared in PBS. 1.25% (w/v) chitosan solution (Chit) was prepared in 0.1 M acetic acid. Monolayer MoS_2 suspension was purchased from Nanjing XFNANO Materials Tech Co., Ltd. All chemicals were of analytical grade without further purification.

Electrochemical measurements were performed with a CHI750E electrochemical working station (Chenhua Apparatus Co., Shanghai, China) with a three-electrode configuration at a steady temperature (25±1 °C). Taking glass carbon electrode (GCE, diameter of 3 mm) as working electrode, platinum and saturated calomel electrode, were employed as an auxiliary electrode and reference electrode, respectively. A magnetic stirrer was used for assisting convection during testing.

2.2. Characterization.

The morphology and structure for the bimetallic nanocomposites were characterized by transmission electron microscopy (TEM), X-ray photoelectron spectrum (XPS) and X-ray diffraction (XRD). TEM images were recorded on a TEM (JEOL JEM-200EX, Japan). XPS was then performed on a Thermo Scientific ESCALAB 250Xi photoelectron spectrometer using Mg-Ka as the exciting source

(1253.6 eV). XRD was recorded with Rigaku D/MAX-2500 powder diffractometer with Cu Ka (λ=0.15406 nm) operated at 40 kV, 200 mA.

2.3. Preparation of bimetallic alloy NWs and PdNi NWs/m-MoS_2

Ultra-thin bimetallic alloy nanowires with three-dimensional porous architecture were synthesized via a surfactant-directed aqueous method [43]. First, appropriate amounts of metal precursors with a total metal ions concentration of 1 M were added into 0.5%wt Triton X-114 aqueous solution. Subsequently, 9 ml of the freshly prepared $NaBH_4$ solution (0.1 M) was rapidly injected into the above solution mixture under magnetic stirring. After 10 min, the resulting black precipitates were centrifuged and washed with absolute ethanol and water at least three times, respectively. Thus, ultra-thin bimetallic alloy nanowires were eventually obtained.

PdNi NWs/m-MoS_2 nanocomposite was prepared as follows. First, 2 ml of MoS_2 suspension (1 mg ml^{-1}) was centrifuged for 30 min and then the obtained black precipitate was re-dispersed in 4 ml aqueous solution containing appropriate amounts of metal precursors, via ultrasonic dispersing technology. Then, 0.5%wt Triton X-114 and freshly prepared $NaBH_4$ solution (0.15 M) were injected into the above solution in sequence, with magnetic stirring. After 10 min of reaction, the resulting solution was centrifuged and washed with absolute ethanol and water at three times. Finally, the PdNi NWs/m-MoS_2 was obtained for further experiments.

2.4. Fabrication of Biosensor System

Initially, GCE was polished with alumina powder (0.3 μm, 50 nm) and then ultrasonically rinsed with ethanol, nitric acid and water, respectively. Then, 10 μl of the suspension of PdNi NWs/m-MoS_2 nanocomposite of desired concentration was coated onto fresh GCE surface and dried at room temperature. Lastly, 1 μl AChE and 5 μl Chit were further spread onto the PdNi NWs/m-MoS_2/GCE and stored at 4°C in a refrigerator before measurements.

2.5. Electrochemical analysis of omethoate

Differential pulse voltammetry (DPV) measurements were used for electrochemical detection of omethoate, via enzymatic inhibition pathway. Exposure to a certain concentration of omethoate, AChE gets phosphorylated thus inhibiting the activity of enzyme, and leading to a decrease of electrochemical oxidation of thiocholine. DPV measurements were recorded at 0.55 V in PBS (0.1 M, pH 7.4) containing 3 mM ATCl. The fabricated biosensor was incubated with different concentrations of omethoate for 15 min. The peak current before omethoate inhibition (I_0) and after inhibition (I_i) were recorded. The inhibition percentage (I%) was calculated as following equation：

$$Inhibition\,(\%) = \left[(I_0 - I_i) / I_0\right] \times 100$$

Furthermore, the calibration curve with a range of linearity was obtained.

3. Results and discussion

3.1. Morphological and structural characterization

The PdNi alloy presents a three-dimensional porous architecture with intertwining nanowires (Fig. S1A, in Supplementary material). These features provide

a promising matrix with exceptionally high electrical conductivity as well as large surface area for electrochemical reaction. Fig. 1A-C are representative transmission electron microscopy (TEM) images of PdNi NWs ($Pd_{47}Ni_{53}$ NWs) under different magnifications. TEM images of PdCu NWs and PdCo NWs are listed in Fig. S1B, C. These high-quality nanowires appear as a reticulate structure with several hundred nanometers in length and an average diameter of 3.0 nm ± 0.5 nm. The high-resolution TEM image (Fig. 1C) illustrates that PdNi NWs are mainly formed by the face-centered cubic (fcc) (111) lattice image with 0.228 nm lattice spacing. The selected area electron diffraction (SAED) patterns exhibit concentric rings related to the (111), (200), (220) and (311) planes of a fcc lattice, which is highly consistent with the following XRD results, indicating that the NWs are highly crystallized. As shown in Fig. 1D, monolayer MoS_2 nanosheets possess a typical ultrathin and wrinkled structure with large surface area. Fig. 1E shows a TEM image of PdNi NWs/m-MoS_2 nanocomposite, indicating that the ultrathin PdNi NWs have been well deposited on the surface of monolayer MoS_2 nanosheets. The crystalline structures of the alloy and monolayer MoS_2 were characterized by XRD (Fig. 1F). As expected, diffraction peaks related to (111), (200), (220) and (311) planes from Pd are obviously observed, and there are no diffraction peaks corresponding to pure Ni or Ni-rich fcc phase, possibly ascribed to the formation of PdNi solid solution. Besides that, all characteristic peaks of PdNi NWs located between fcc crystal nanostructure of pure Pd (JCPDS no. 46-1043, magenta) and Ni (JCPDS no. 65-2865) peaks, demonstrating the successful formation of PdNi alloy. In addition, characteristic peaks in connection with (002), (100), (103) and (110) planes of MoS_2 (JCPDS no.37-1492) were observed in Fig. 1G. The XPS results are depicted in Fig. 1H and Fig. 1I to further confirm the alloy composition and electronic state. The XPS data demonstrates that alloying of Pd with Ni has successfully changed electronic structure.

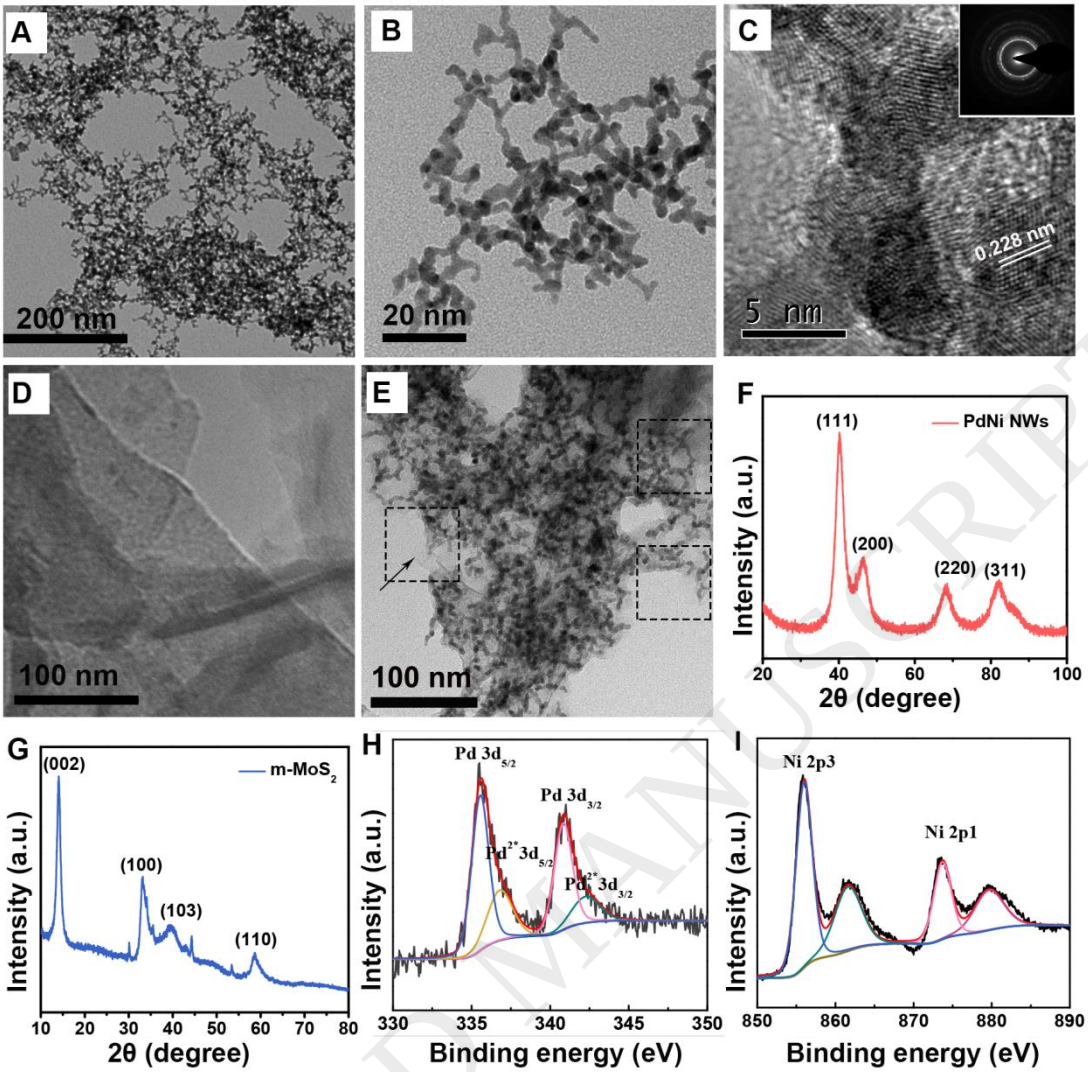

Fig. 1 (A, B) TEM images of PdNi NWs ($Pd_{47}Ni_{53}$ NWs). (C) High-resolution TEM image and SAED patterns of PdNi NWs. (D) TEM image of monolayer MoS_2 nanosheet. (E) TEM image of PdNi NWs/m-MoS_2 nanocomposite (black square marked the edge of MoS_2). (F) XRD patterns of PdNi NWs. (G) XRD patterns of MoS_2. (H) and (I) XPS spectra of Pd3d and Ni2p.

3.2. Electrochemical behavior of modified electrodes

The change of interfacial properties of different modified electrodes was investigated by electrochemical measurements such as cyclic voltammetry (CV) and electrochemical impedance spectroscopy (EIS). Fig. 2A shows typical CV curves of bare GCE, PdCu NWs/GCE, PdCo NWs/GCE, PdNi NWs/GCE and PdNi NWs/m-MoS_2/GCE, in 1.0 M KCl containing 5.0 mM $K_3[Fe(CN)_6]/K_4[Fe(CN)_6]$ (1 : 1) at a scan rate of 100 $mV \cdot s^{-1}$. All curves show a couple of well-defined reversible redox peaks, which relate to Fe^{3+}/Fe^{2+} redox. For bare GCE (curve a), PdCo NWs (curve b) and PdCu NWs (curve c), the curves show broad redox peaks with the peak potential separation (ΔEp) of 0.27 V, 0.191 V and 0.165 V, respectively. In contrast, with the modification of PdNi NWs, the redox currents dramatically increased and ΔEp decreased to 0.121 V (curve d), due to the high electrical conductivity of PdNi

NWs. When incorporation with PdNi NWs/m-MoS_2, the redox currents continue increased and peak potential shifted, with a smallest peak-to-peak ΔEp of 0.101 V (curve e), which revealed that electron transfer at the PdNi NWs/m-MoS_2/GCE is much faster and easier.

Electroactive surface area (A) is a dominating critical factor of nanomaterials, which decides their performance in electrochemical sensors [44]. The electroactive surface area was evaluated by CV measurements at PdNi NWs/m-MoS_2/GCE over a range of scan rate from 10 $mV \cdot s^{-1}$ to 180 $mV \cdot s^{-1}$ in 0.1 M KCl solution containing 5 mM $[Fe(CN)_6]^{3-/4-}$ (Fig. 2B). As shown in Fig. 2B, with the increasing of scan rate from 10 $mV \cdot s^{-1}$ to 180 $mV \cdot s^{-1}$, anodic as well as cathodic peak currents increased, and peak potential obviously shifted, generating a gradually increasing peak-to-peak potential separation. Moreover, the plots of both anodic peak current (I_{pa}) and cathodic peak current (I_{pc}) are in proportion to the square root of scan rate ($\upsilon^{1/2}$), respectively. According to the Randles–Sevcik equation [45], the active surface area of PdNi NWs/m-MoS_2/GCE was calculated as 0.43 cm^2 (in Supplementary material, S2), which is approximately 6-fold of bare GCE (A_{GCE} = 0.0707 cm^2) and larger than 0.146 cm^2 [4], 0.1078 cm^2 [30] and 0.214 cm^2 [46]. It demonstrated that the as-prepared nanomaterials could be an ideal candidate with large surface area for electrochemical reaction.

Another key factor that greatly impact their performance for electroanalytical applications associates with the electron transfer ability of the nanocomposites in electrochemical reactions [44]. EIS was performed to evaluate this ability using $[Fe(CN)_6]^{3-/4-}$ as a redox probe. In Fig 2C, Nyquist plots of bare GCE or different modified electrodes were obtained, including a semicircle section at higher frequencies correlated with electron-transfer-limited process and a linear portion at lower frequency related to diffusion-limited process. Electron-transfer resistance (Ret), calculated as the diameter of the semicircle section, reflects the electron-transfer kinetics of the redox process at the electrodes surface. As shown in Fig 2C, compared to the bare GCE (curve a), PdCo NWs/GCE (curve b), PdCu NWs/GCE (curve c) and PdNi NWs/GCE (curve d), PdNi NWs/m-MoS_2/GCE (curve e) shows a significantly smaller semicircle and outperforms other four electrodes, attributed to the inherent high electrical conductivity and synergistic signal amplification effect. Our results proved that PdNi NWs/m-MoS_2 nanocomposite with high conductivity could serve as an excellent transducer to promote electron transfer in electrochemical reactions. In addition, the calculational results of Ret at bare GCE, PdCu NWs/GCE, PdCo NWs/GCE, PdNi NWs/GCE and PdNi NWs/m-MoS_2/GCE are shown in Fig. 2D.

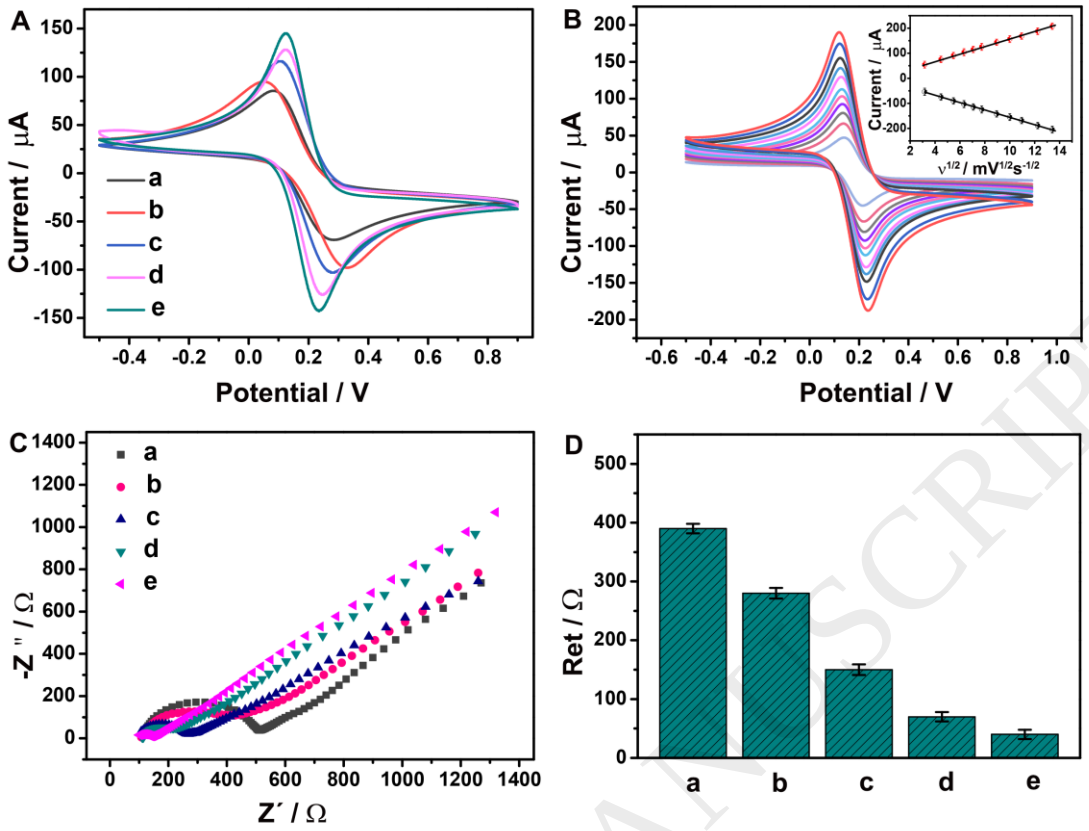

Fig. 2 (A) Cyclic voltammetry curves of (a) bare GCE, (b) PdCo NWs/GCE, (c) PdCu NWs/GCE, (d) PdNi NWs/GCE, (e) PdNi NWs/m-MoS_2/GCE in 1.0 M KCl containing 5.0 mM $K_3[Fe(CN)_6]/K_4[Fe(CN)_6]$ (1 : 1) at scan rate of 100 $mV \cdot s^{-1}$. (B) Cyclic voltammetry curves of PdNi NWs/m-MoS_2/GCE at scan rate from 10 $mV \cdot s^{-1}$ to 180 $mV \cdot s^{-1}$ (a-k). Inset B, Plots of peak current vs square root of scan rate ($\nu^{1/2}$). (C) Nyquist plots of bare and modified electrodes in 0.1 M KCl solution containing 5 mM $[Fe(CN)_6]^{3-/4-}$. (D) The histogram for charge transfer resistance (Ret) of bare and modified electrodes. Error bars are coefficient of variation across three repetitive experiments.

3.3. Optimization of Experimental Conditions.

For the sake of highly sensitive detection of pesticides, several fabricated conditions were optimized. The amount of Chit is an important component in the construction of biosensor, which serves as a positively charged interface for the immobilization of the negatively charged AChE. Five different amounts (2 µl, 5 µl, 8 µl, 10 µl, and 15 µl) were studied. Low amounts of Chit may cause the AChE leakage, while high amounts of Chit could reduce conductivity and obstruct the transfer of electronics. As shown in Fig. 3A, the optimum amount of Chit was obtained as 5 µl.

Apart from the amount of Chit, different ratios of PdNi NWs, PdCu NWs, PdCo NWs have an important effect on the properties. Four different ratios of Pd/non-noble metals (3:1, 2:1, 1:1 and 1:2) of the NWs were investigated. As can be seen in Fig. 3B, the current responses of Pd_1Ni_1 NWs, Pd_1Co_1 NWs and Pd_1Cu_2 NWs were obtained to be the maximum value. Hence, 1:1, 1:1 and 1:2 were chosen as the optimal ratios of PdNi NWs, PdCo NWs, PdCu NWs for subsequent experiments, respectively.

Furthermore, the concentration of PdNi NWs/m-MoS_2 nanocomposite also plays an essential role in the sensing performance. Four different concentrations (0.5, 1, 5, and 10 mg mL^{-1}) were investigated. In Fig. 3C, the current value intensified with a monotonically increasing of the concentration from 0.5 mg mL^{-1} to 1 mg mL^{-1}, and then sharply dropped over 1 mg mL^{-1}. A proper concentration of the PdNi NWs/m-MoS_2 nanocomposite could efficiently facilitate electron transfer and enhance the electrochemical performance in the sensing process. Conversely, high concentrations may lead to excess PdNi NWs/m-MoS_2 nanocomposite deposited, generating a barrier and hindering electron transfer. Hence, 1 mg mL^{-1} PdNi NWs/m-MoS_2 was employed to fabricate the electrodes.

In addition, the incubation time to the enzyme has a significant impact on the performance of the biosensor. As can be seen in Fig. 3D, the inhibition percentage gradually increased as the incubation time increased from 5 to 15 min, and tended to be stable after 15 min. The results indicated that the binding equilibrium of omethoate molecules with the AChE binding sites. In consideration of high efficiency, 15 min was chosen as the optimal incubation time for the subsequent experiments.

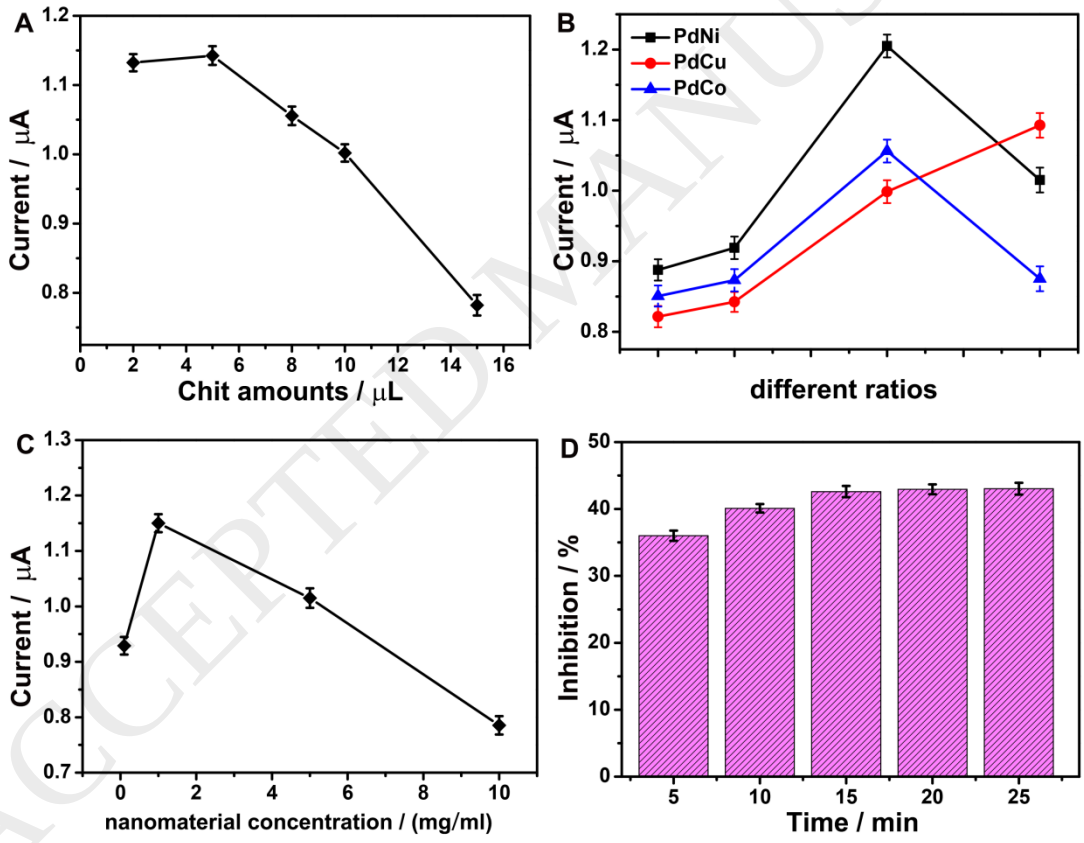

Fig. 3. Effect of (A) Chit amounts, (B) different ratios of PdNi NWs, PdCu NWs, PdCo NWs, (C) the concentration of PdNi NWs/m-MoS_2 nanocomposite, (D) inhibition time on the responses of the biosensor. Error bars are coefficient of variation across three repetitive experiments.

3.4 Amperometric response toward ATCl.

It is of utmost interest to investigate the responses of biosensors towards ATCl

based on different bimetallic alloy nanocomposites (PdCo NWs, PdCu NWs, PdNi NWs and PdNi NWs/m-MoS_2). The current-time amperometric measurements were carried out to evaluate the responses of different biosensors by successive additions of the same concentration of ATCl (Fig. 4A). As can be seen in Fig. 4A, AChE-Chit/PdNi NWs/m-MoS_2/GCE shows more superior performances in comparison to other corresponding biosensors based on PdCo NWs, PdCu NWs, and PdNi NWs. The results are attributed to that the PdNi NWs/m-MoS_2 nanocomposite on the sensing platform could not only efficiently accelerate electron transfer between the electrode and electroactive substances, but also create synergetic effect to improve electrochemical performance. Fig. 4B shows the amperometric responses of AChE-Chit/PdNi NWs/m-MoS_2/GCE by successive addition of a series of concentrations of ATCl. The oxidation current increases with ATCl concentration and tends to be stable in the high concentration, suggesting that accord the dynamical character of enzymatic reactions (Fig. 4C). The calibration equation is I= 1.148C+ 0.0463 (R^2 = 0.998, n=3), where I represents the oxidation current (μA) and C represents ATCl concentration (mM) (Fig. 4D). It shows a good liner relationship between I and C, with a wide range of 0.01 mM~1.0 mM. The sensitivity was calculated as 1.148 μA·mM^{-1}. In order to further verify the affinity of the AChE to ATCl, Michaelis-Menten constant (K_m), was calculated by the Lineweaver–Burk equation [47], which is inversely proportional to the affinity. The K_m value for this as-prepared biosensor was 62.6 μM, which is significantly smaller than 106 μM [48], 131μM [49] and 3.1 mM [47] reported in previous reports. The results indicate that the AChE immobilized on PdNi NWs/m-MoS_2/GCE has a high affinity towards ATCl.

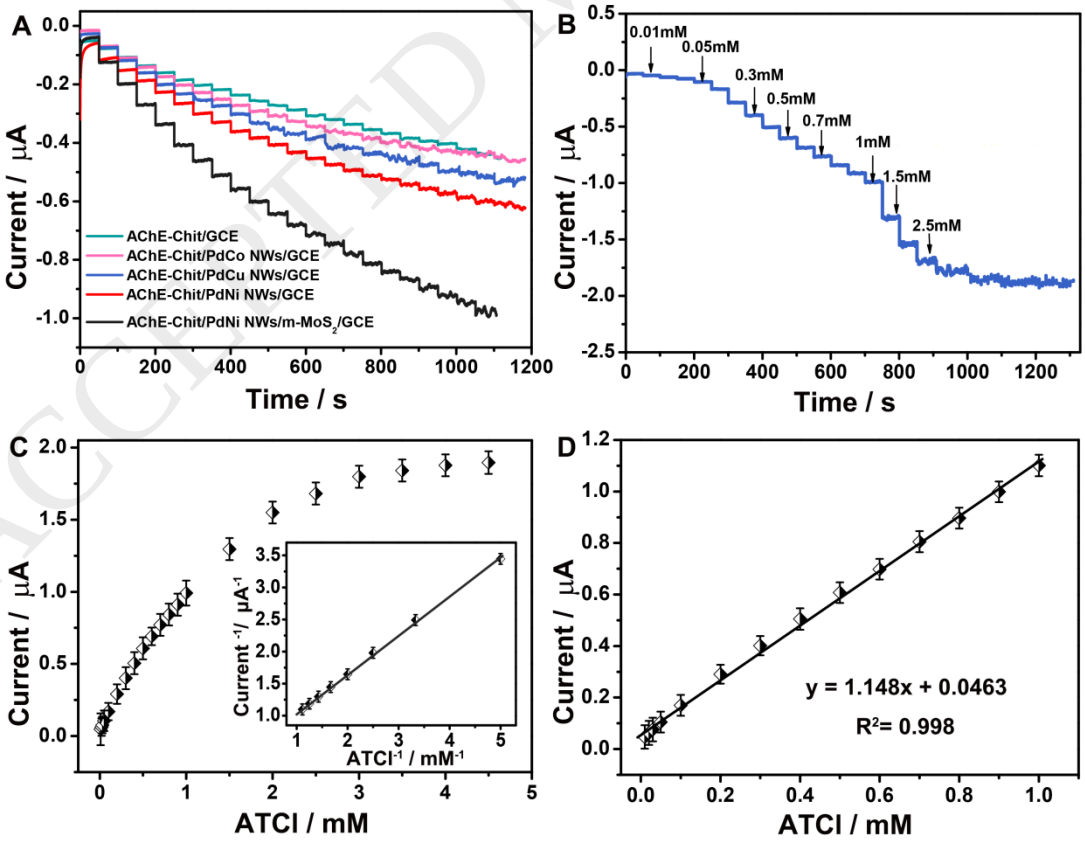

Fig. 4. (A) Amperometric responses of AChE-Chit/GCE, AChE-Chit/PdCo NWs/GCE, AChE-Chit/PdCu NWs/GCE, AChE-Chit/PdNi NWs/GCE and AChE-Chit/PdNi NWs/m-MoS_2/GCE by successive addition of ATCl with the same concentration in 0.1 M PBS with a mild stirring; applied potential: 0.55 V vs Ag/AgCl. (B) Amperometric response of the PdNi NWs/m-MoS_2/GCE by successive addition of ATCl with varying concentrations in 0.1 M PBS with a mild stirring. (C) Relationship between the current and ATCl concentration. Inset c shows the Lineweaver-Burk plot of 1/Iss vs. 1/C. (D) show the calibration curve for ATCl determination. Error bars are coefficient of variation across three repetitive experiments.

3.5. Omethoate Detection.

Omethoate, as a representative organophosphate pesticide, was chosen as model inhibitor. Under the optimized experimental conditions, AChE-Chit/PdNi NWs/m-MoS_2/GCE was employed for the detection of omethoate to verify the performance of this sensing platform. DPV responses of different concentrations of omethoate are illustrated in Fig. 5A. As what can be seen in Fig. 5B, a certain linear relationship meets between the inhibition percentage (I%) and logarithm of the omethoate concentration (lg C) over a range from 10^{-13} M to 10^{-7} M. The linear regression equation for omethoate is y= 3.57 x+ 57.81, with a correlation coefficient (R^2) of 0.998. By using the 3 S/N principle, the limit of detection (LOD) for omethoate was obtained as 0.05 pM. In comparison with previous literature [14,50,51], this biosensor showed superior performances, including a broader linear range and a lower limit of detection. The comparative results were listed in Table 1. In addition, the obtained LOD far exceeds the maximum residue limits (MRLs) for omethoate (200 μg/L) set by European Union. To date, according to the literature, the general concentration range of pesticide pollutant is about 1 pM ~ 0.1 μM [17] [52]. The remarkable performances of the proposed biosensor are ascribed to the signal amplification effect between PdNi NWs and monolayer MoS_2 nanosheet. The PdNi NWs/m-MoS_2 nanocomposite has large surface area, excellent conductivity and biocompatibility, which not only could provide large area and accelerate electron transfer in electrochemical reactions, but also create a favorable biological environment.

The fabricated biosensor was employed to determine omethoate in commercial vegetable samples purchased from a local market and prepared by a Chinese Official Standard Method (in Supplementary material, S4). The results were listed in Table S1. The recoveries were in the range of 90.4%-96.1% and the RSDs were below 5%, indicating that the AChE-Chit/PdNi NWs/m-MoS_2 biosensor was reliable for the determination of omethoate in real samples.

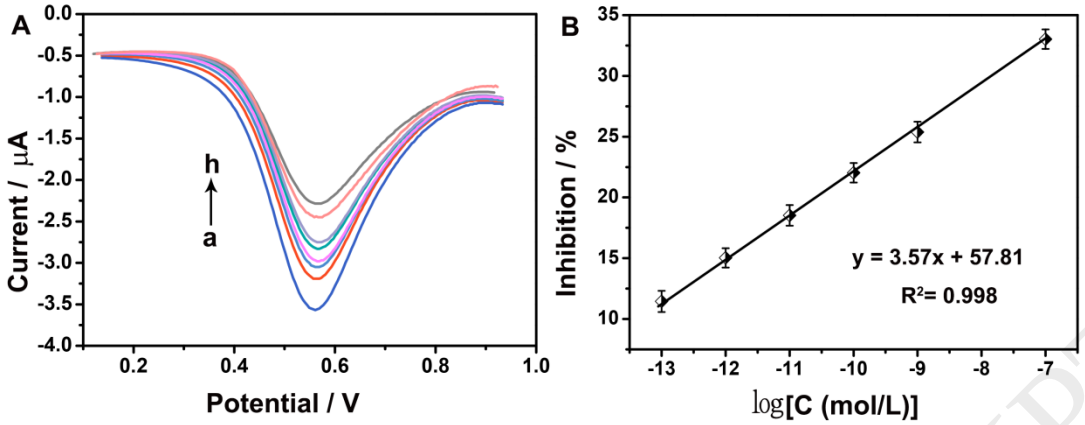

Fig. 5 (A) DPV responses of AChE-Chit/PdNi NWs/m-MoS_2/GCE in 0.1 M pH 7.4 PBS solution with 3 mM ATCl after incubation in (A) a-h: 0, 10^{-13}, 10^{-12}, 10^{-11}, 10^{-10}, 10^{-9}, 10^{-7} and 10^{-6} M of omethoate for 15 min (B) Calibration curves for omethoate determination. Error bars are coefficient of variation across three repetitive experiments.

3.6. Repeatability, reproducibility, stability and interference studies

To evaluate the repeatability of the proposed biosensor, five successive DPV measurements of the AChE-Chit/PdNi NWs/m-MoS_2/GCE were carried out. Relative standard deviation (RSD) was obtained as 2.7%, indicating a good repeatability of this method. In addition, the as-prepared biosensor shows good reproducibility with a RSD of 3.1% tested by DPV measurements of five independently electrodes under the same conditions. The long-time stability of the biosensor was investigated for 30 consecutive days. The AChE-Chit/PdNi NWs/m-MoS_2 modified electrodes were stored in a refrigerator keeping 4 °C for further use. After a week, the current responses of the biosensor retained approximately 92% of its origin value. After 30 days, DPV responses reduced by 9.5% of its origin value. The results reveal that the biosensor has an excellent stability for the further practical application. Some electroactive interference substances such as glucose, ascorbic acid, phenol, catechol, Zn^{2+}, Mg^{2+}, Cl^- and NO_3^-, were selected as control samples to evaluate their effects on the performance of the biosensor and verify the specificity of the proposed biosensor. Despite the concentrations of these interferents were higher than ATCl, there were no obvious change in Fig. S2. The result demonstrated that biosensor on the basis of AChE-Chit/PdNi NWs/m-MoS_2 could selectively detect omethoate in the presence of these common interfering species normally existed in the food and environment.

Conclusion

In this work, a highly sensitive and effective electrochemical detection platform for omethoate has been successfully developed based on PdNi NWs/m-MoS_2 nanocomposite, through enzymatic inhibition pathway. All three reported bimetallic alloy NWs enhanced the responses of the AChE biosensor and PdNi NWs outperformed PdCu NWs and PdCo NWs. Besides that, PdNi NWs/m-MoS_2 as a sensing platform shows more superior performance than the corresponding biosensor

without monolayer MoS_2 nanosheet under the same condition. The PdNi NWs/m-MoS_2 nanocomposite possesses excellent conductivity as well as large active surface area, which could not only serve as a prominent transducer to promote electron transfer in electrochemical reactions, but also increase catalytic sites for electrochemical oxidation of ATCl. Under optimal conditions, the proposed biosensor shows outstanding sensing performance for monitoring omethoate with high sensitivity, wide linear range (10^{-13} M~10^{-7} M) and a low detection limit of 0.05 pM. Moreover, the proposed biosensor exhibited long-time stability, high specificity, good reproducibility and recovery rates. The construction of this novel sensing platform holds great potentials in the on-site analysis of pesticide residues in the field of food security and environmental measurement.

Acknowledgments

The authors acknowledge the financial support from the National Natural Science Foundation of China (Grant No. 21371149, 21671168) and the Natural Science Foundation of Hebei (Grant No. B2016203498, 17964403D)

References

[1]. J.M. Abad, F. Pariente, L. Herna´ndez, H.D. Abrun˜a, E. Lorenzo, Determination of organophosphorus and carbamate pesticides using a piezoelectric biosensor, Anal. Chem. 70 (1988) 2848-2855.

[2]. A. Mulchandani, W. Chen, P. Mulchandani, J. Wang, K. Rogers, Biosensors for direct determination of organophosphate pesticides, Biosens. Bioelectron. 16 (2001) 225–230.

[3]. A.A. Ciucu, C. Negulescu, R.P. Baldwin, Detection of pesticides using an amperometric biosensor based on ferophthalocyanine chemically modified carbon paste electrode and immobilized bienzymatic system, Biosens. Bioelectron. 18 (2003) 303–310.

[4]. Y.B. Zeng, D.J. Yu, Y.Y. Yu, T.S. Zhou, G.Y. Shi, Differential pulse voltammetric determination of methyl parathion based on multiwalled carbon nanotubes–poly(acrylamide) nanocomposite film modified electrode, J. Hazard. Mater. 217–218 (2012) 315–322.

[5]. D.M. Quinn, Acetylcholinesterase: enzyme structure, reaction dynamics, and virtual transition states, Chem. Rev. 87 (1987) 955−979.

[6]. H.D. Cancar, S. Soylemez, Y. Akpinar, M. Kesik, S. Göker, G. Gunbas, M. Volkan and L. Toppare, A novel acetylcholinesterase biosensor: core–shell magnetic nanoparticles incorporating a conjugated polymer for the detection of organophosphorus pesticides, ACS Appl. Mater. Interfaces 8 (2016) 8058–8067.

[7]. G.Z. Liu, W.Q. Guo, Z. Yin, Covalent fabrication of methyl parathion hydrolase on gold nanoparticles modified carbon substrates for designing a methyl parathion biosensor, Biosens. Bioelectron. 53 (2014) 440−446.

[8]. N. Chauhan, J. Narang and C.S. Pundir, Immobilization of rat brain acetylcholinesterase on ZnS and poly(indole-5-carboxylic acid) modified Au electrode for detection of organophosphorus insecticides. Biosens. Bioelectron. 29 (2011), 82–88.

[9]. K. Zhang, Q.S. Mei, G.J. Guan, B.H. Liu, S.H. Wang, Z.P. Zhang, Ligand replacement-induced fluorescence switch of quantum dots for ultrasensitive detection of organophosphorothioate pesticides, Anal. Chem. 82 (2010) 9579−9586.

[10]. G.H. Yao, R.P. Liang, C.F. Huang, Y. Wang, J.D. Qiu, Surface plasmon resonance sensor based on magnetic molecularly imprinted polymers amplification for pesticide recognition, Anal. Chem. 85 (2013) 11944−11951.

[11]. H. Wang, J. Wang, C. Timchalk, Y. Lin, Magnetic electrochemical immunoassays with quantum dot labels for detection of phosphorylated acetylcholinesterase in plasma, Anal. Chem. 80 (2008) 8477−8484.

[12]. M.U.A. Prathap, A.K. Chaurasia, S.N. Sawant, S.K. Apte, Polyaniline-based highly sensitive microbial biosensor for selective detection of lindane, Anal. Chem. 84 (2012) 6672−6678

[13]. J. Hassana, A. Farahani, M. Shamsipur, F. Damerchili, Rapid and simple low density miniaturized homogeneous liquid–liquid extraction and gas chromatography/mass spectrometric determination of pesticide residues in sediment, J. Hazard. Mater. 184 (2010) 869−871.

[14]. Z.Z. Zheng, Y.L. Zhou, X.Y. Li, S.Q. Liu, Z.Y. Tang, Highly-sensitive organophosphorous pesticide biosensors based on nanostructured films of acetylcholinesterase and CdTe quantum dots, Biosens. Bioelectron. 26 (2011) 3081–3085.

[15]. J. Bao, C.J. Hou, M. Chen, J.J. Li, D.Q. Huo, M. Yang, X.G. Luo, Y. Lei, Plant esterase–chitosan/gold nanoparticles–graphene nanosheet composite-based biosensor for the ultrasensitive detection of organophosphate pesticides, J. Agric. Food Chem. 63 (2015) 10319–10326.

[16]. J. Kirsch, C. Siltanen, Q. Zhou, A. Revzin, A. Simonian, Biosensor technology: recent advances in threat agent detection and medicine, Chem. Soc. Rev. 42 (2013) 8733–8768.

[17]. D.D. Song, Y.Z. Wang, X. Lu, Y.K. Gao, Y. Li, F.M. Gao, Ag nanoparticles-decorated nitrogen-fluorine co-doped monolayer MoS_2 nanosheet for highly sensitive electrochemical sensing of organophosphorus pesticides, Sens. Actuators B: Chem 267 (2018) 5–13.

[18]. S. Kurbanoglu, S.A. Ozkan, A. Merkoci, Nanomaterials-based enzyme electrochemical biosensors operating through inhibition for biosensing applications, Biosens. Bioelectron. 89 (2017) 886–898.

[19]. C.Z. Zhu, G.H. Yang, H. Li, D. Du, Y.H. Lin, Electrochemical sensors and biosensors based on nanomaterials and nanostructures, Anal. Chem. 87 (2015) 230−249.

[20]. X. Lu, L. Tao, D.D. Song, Y. Li, F.M. Gao, Bimetallic Pd@Au nanorods based ultrasensitive acetylcholinesterase biosensor for determination of organophosphate pesticides, Sens. Actuators B: Chem 255 (2018) 2575−2581.

[21]. Z.H. Hu, Z.T. Wu, J. He, Z.H. Ni, W. Chen, Two-dimensional transition metal dichalcogenides: interface and defect engineering, Chem. Soc. Rev. 47 (2018) 3100–3128.

[22]. J. Feng, X. Sun, C.Z. Wu, L.L. Peng, C.W. Lin, S.L. Hu, J.L. Yang, Y. Xie, Metallic few-layered VS_2 ultrathin nanosheets: high two-dimensional conductivity for in-plane supercapacitors, J. Am. Chem. Soc. 133 (2011) 17832–17838.

[23]. X. Huang, Z.Y. Zeng, H. Zhang, Metal dichalcogenide nanosheets: preparation, properties

and applications, Chem. Soc. Rev. 42 (2013) 1934–1946.

[24]. W. Chen, J. Zhao, J. Zhang, L. Gu, Z.Z. Yang, X.M. Li, H. Yu, X.T. Zhu, R. Yang, D.X. Shi, X.C. Lin, J.D. Guo, X.D. Bai, Oxygen-assisted chemical vapor deposition growth of large single-crystal and high-quality monolayer MoS_2, J. Am. Chem. Soc. 137 (2015) 15632−15635.

[25]. X.M. Geng, Y.L. Zhang, Y. Han, J.X. Li, L. Yang, M. Benamara, L. Chen, H.L. Zhu, Two-dimensional water-coupled metallic MoS_2 with nanochannels for ultrafast supercapacitors, Nano Lett. 17 (2017) 1825−1832.

[26]. H. Rezaei, S.J. Ardakani, K.J. Smith, Comparison of MoS_2 catalysts prepared from Mo-micelle and Mo-octoate precursors for hydroconversion of cold lake vacuum residue: catalyst activity, coke properties and catalyst recycle, Energy Fuels 26 (2012) 2768–2778.

[27]. M.Z.M. Nasir, C.C. Mayorga-Martinez, Z. Sofer and M. Pumera, Two-dimensional 1T-phase transition metal dichalcogenides as nanocarriers to enhance and stabilize enzyme activity for electrochemical pesticide detection, ACS Nano. 11 (2017) 5774−5784.

[28]. C.L. Tan, H. Zhang, Two-dimensional transition metal dichalcogenide nanosheet-based composites, Chem. Soc. Rev. 44 (2015) 2713–2731.

[29]. X.R. Gan, H.M. Zhao, X. Quan, Two-dimensional MoS_2: A promising building block for biosensors, Biosens. Bioelectron. 89 (2017) 56–71.

[30]. Y.Y. Zhang, M.A. Arugula, M. Wales, J. Wild, A novel layer-by-layer assembled multi-enzyme/CNT biosensor for discriminative detection between organophosphorus and non-organophosphrus pesticides, Biosens. Bioelectron. 67 (2015) 287–295.

[31]. C.H. Naylor, N.J. Kybert, C. Schneier, J. Xi, G. Romero, J.G. Saven, R. Liu, A.T.C. Johnson, Scalable production of molybdenum disulfide based biosensors, ACS Nano. 10 (2016) 6173−6179.

[32]. F.K. Perkins, A.L. Friedman, E. Cobas, P.M. Campbell, G.G. Jernigan, B.T. Jonker, Chemical vapor sensing with monolayer MoS_2, Nano Lett. 13 (2013) 668−673.

[33]. S.X. Wu, Z.Y. Zeng, Q.Y. He, Z.J. Wang, S.J. Wang, Y.P. Du, Z.Y. Yin, X.P. Sun, W. Chen, H. Zhang, Electrochemically reduced single-layer MoS_2 nanosheets: characterization, properties, and sensing applications, Small. 8 (2012) 2264−2270.

[34]. S. Xu, D. Li, P. Wu, One-pot, facile, and versatile synthesis of monolayer MoS_2/WS_2 quantum dots as bioimaging probes and efficient electrocatalysts for hydrogen evolution reaction, Adv. Funct. Mater. 25 (2015) 1127–1136.

[35]. J. Yang, S. Deng, J. Lei, H. Ju, S. Gunasekaran, Electrochemical synthesis of reduced graphene sheet–AuPd alloy nanoparticle composites for enzymatic biosensing Biosens.Bioelectron. 29 (2011) 159–166.

[36]. T.D. Thanh, J. Balamurugan, S.H. Lee, N.H. Kim, J.H. Lee, Novel porous gold-palladium nanoalloy network-supported graphene as an advanced catalyst for non-enzymatic hydrogen peroxide sensing, Biosens. Bioelectron. 85 (2016) 669–678.

[37]. J.L. Fernández, V., Raghuveer, A. Manthiram, A.J. Bard, Pd−Ti and Pd−Co−Au electrocatalysts as a replacement for platinum for oxygen reduction in proton exchange membrane fuel cells, J. Am. Chem. Soc. 127 (2005) 13100−13101.

[38]. L.Y. Chen, H. Guo, T. Fujita, A. Hirata, W. Zhang, A. Inoue, M.W. Chen, Nanoporous PdNi bimetallic catalyst with enhanced electrocatalytic performances for electro-oxidation and oxygen reduction reactions, Adv. Funct. Mater. 21 (2011) 4364–4370.

[39]. C.Y. Du, M. Chen, W.G. Wang, G.P. Yin, A highly stable acetylcholinesterase biosensor based on chitosan-TiO_2-graphene nanocomposites for detection of organophosphate pesticides, ACS Appl. Mater. Interfaces. 3 (2011) 105–109.

[40]. Z.Y. Shih, C.W. Wang, G. Xu, H.T. Chang, Porous palladium copper nanoparticles for the electrocatalytic oxidation of methanol in direct methanol fuel cells, J. Mater. Chem. A. 1 (2011) 4773−4778.

[41]. L. Shang, F.Q. Zhao, B.Z. Zeng, 3D porous graphene–porous PdCu alloy nanoparticles–molecularly imprinted poly(para-aminobenzoic acid) composite for the electrocatalytic assay of melamine, ACS Appl. Mater. Interfaces. 6 (2014) 18721−18727.

[42]. J.J. Willis, E.D. Goodman, L.F. Wu, A.R. Riscoe, P. Martins, C.J. Tassone, M. Cargnello, Systematic identification of promoters for methane oxidation catalysts using size- and composition-controlled pd-based bimetallic nanocrystals, J. Am. Chem. Soc. 139 (2017) 11989−11997.

[43]. X. Zhao, J. Zhang, L.J. Wang, H.X. Li, Z.L. Liu, W. Chen, Ultrathin PtPdCu Nanowires Fused Porous Architecture with 3D Molecular Accessibility: An Active and Durable Platform for Methanol OxidationACS Appl. Mater. Interfaces. 7 (2015) 26333−26339.

[44]. C.L. Tan, X.H. Cao, X.J. Wu, Q.Y. He, J. Yang, X. Zhang, J. Chen, W. Zhao, S.K. Han, G.H. Nam, M. Sindoro, H. Zhang, Recent advances in ultrathin two-dimensional nanomaterials, Chem. Rev. 117 (2017) 6225−6331.

[45]. D.G. Rackus, M.H. Shamsi, A.R. Wheeler, Electrochemistry, biosensors and microfluidics: a convergence of fields, Chem. Soc. Rev. 44 (2015) 5320−5340.

[46]. C. Ye, M.Q. Wang, X. Zhong, S.H. Chen, Y.Q. Chai, R. Yuan, Highly sensitive electrochemiluminescenc assay of acetylcholinesterase activity based on dual biomarkers using Pd–Au nanowires as immobilization platform, Biosens. Bioelectron. 79 (2016) 34−40.

[47]. H.F. Cui, W.W. Wu, M.M. Li, X.J. Song, Y.X. Lv, T.T. Zhang, A highly stable acetylcholinesterase biosensor based on chitosan-TiO_2-graphene nanocomposites for detection of organophosphate pesticides, Biosens. Bioelectron. 99 (2018) 223–229.

[48]. H.Y. Zhao, X.P. Ji, B.B. Wang, N. Wang, X.R. Li, R.X. Ni and J.J. Ren, An ultra-sensitive acetylcholinesterase biosensor based on reduced graphene oxide-Au nanoparticles-β-cyclodextrin/prussian blue chitosan nanocomposites for organophosphorus pesticides detection, Biosens. Bioelectron. 65 (2015) 23–30.

[49]. Q. Zhou, L. Yang, G.C. Wang and Y. Yang, Acetylcholinesterase biosensor based on SnO_2 nanoparticles-carboxylic graphene-nafion modified electrode for detection of pesticides. Biosens. Bioelectron. 49 (2013) 25–31.

[50]. B. Bucur, M. Dondoi, A. Danet, J.L. Marty, Insecticide identification using a flow injection analysis system with biosensors based on various cholinesterases, Anal. Chim. Acta. 539 (2005) 195–201.

[51]. X. Sun and X.Y. Wang, Acetylcholinesterase biosensor based on prussian blue-modified electrode for detecting organophosphorous pesticides. Biosens. Bioelectron. 25 (2010) 2611–2614.

[52]. C.S. Pundir and N. Chauhan, Acetylcholinesterase inhibition-based biosensors for pesticide determination: A review, Anal. Biochem. 429 (2012) 19–31.

Table 1 Comparisons of the as-prepared biosensors with other biosensors for the determination of omethoate.

Biosensors	Linear range	Detection limit	Immobilization method of AChE	Detection method	Inhibition time	References
PAH/CdTe QDs/AChE	1 pM−1 μM	58.9 pM	Electrostatic interaction	fluorescent detection	15 min	[14]
Dm-AChE/SPE	0.1−50 μM	0.1 μM	Entrapment	Amperometric	15 min	[50]
AChE-PB/GCE	50 ng/L−10 μg/L	15 ng/L	Glutaraldehyde crosslinking	Amperometric	10 min	[51]
AChE-Chit/PdNi NWs/m-MoS_2/GCE	10^{-13} M~10^{-7} M	0.05 pM	Covalent	DPV	15 min	This work